Structural Basis for Different Substrate Profiles of Two Closely Related Class D β-Lactamases and Their Inhibition by Halogens

Vlatko Stojanoski,[†,‡] Dar-Chone Chow,[‡] Bartlomiej Fryszczyn,[†,‡] Liya Hu,[†] Patrice Nordmann,[§] Laurent Poirel,[§] Banumathi Sankaran,[∥] B. V. Venkataram Prasad,[†] and Timothy Palzkill*[,†,‡]

[†]Verna and Marrs McLean Department of Biochemistry and Molecular Biology and [‡]Department of Pharmacology, Baylor College of Medicine, Houston, Texas 77030, United States

[§]Medical and Molecular Microbiology "Emerging Antibiotic Resistance" Unit, Department of Medicine, Faculty of Science, University of Fribourg, 1700 Fribourg, Switzerland

[∥]Berkeley Center for Structural Biology, Advanced Light Source, Lawrence Berkeley National Laboratory, Berkeley, California 94720, United States

ABSTRACT: OXA-163 and OXA-48 are closely related class D β-lactamases that exhibit different substrate profiles. OXA-163 hydrolyzes oxyimino-cephalosporins, particularly ceftazidime, while OXA-48 prefers carbapenem substrates. OXA-163 differs from OXA-48 by one substitution (S212D) in the active-site β5 strand and a four-amino acid deletion (214-RIEP-217) in the loop connecting the β5 and β6 strands. Although the structure of OXA-48 has been determined, the structure of OXA-163 is unknown. To further understand the basis for their different substrate specificities, we performed enzyme kinetic analysis, inhibition assays, X-ray crystallography, and molecular modeling. The results confirm the carbapenemase nature of OXA-48 and the ability of OXA-163 to hydrolyze the oxyimino-cephalosporin ceftazidime. The crystal structure of OXA-163 determined at 1.72 Å resolution reveals an expanded active site compared to that of OXA-48, which allows the bulky substrate ceftazidime to be accommodated. The structural differences with OXA-48, which cannot hydrolyze ceftazidime, provide a rationale for the change in substrate specificity between the enzymes. OXA-163 also crystallized under another condition that included iodide. The crystal structure determined at 2.87 Å resolution revealed iodide in the active site accompanied by several significant conformational changes, including a distortion of the β5 strand, decarboxylation of Lys73, and distortion of the substrate-binding site. Further studies showed that both OXA-163 and OXA-48 are inhibited in the presence of iodide. In addition, OXA-10, which is not a member of the OXA-48-like family, is also inhibited by iodide. These findings provide a molecular basis for the hydrolysis of ceftazidime by OXA-163 and, more broadly, show how minor sequence changes can profoundly alter the active-site configuration and thereby affect the substrate profile of an enzyme.

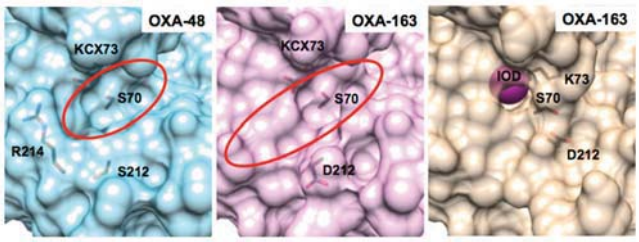

β-Lactams are the most commonly prescribed antibiotics worldwide.[1] Therefore, bacterial resistance toward these drugs presents a serious public health threat.[2,3] The effectiveness of β-lactam antibiotics is challenged by the emergence of multidrug resistant Gram-negative bacteria from the Enterobacteriaceae family such as *Klebsiella pneumoniae*.[4−7] The most common mechanism of β-lactam antibiotic resistance in Gram-negative pathogens is the production of β-lactamases that hydrolyze and inactivate the drugs.[8−11] β-Lactamases are divided into four classes (A−D) based on amino acid sequence homology.[12] Class A, C, and D enzymes are serine hydrolases, while members of class B are metallo-β-lactamases that are unrelated in sequence and mechanism to the other classes.[12,13] In recent years, β-lactamase variants from classes A and D with the ability to hydrolyze oxyimino-cephalosporins and carbapenems have emerged. This alarming trend is reducing the number of treatment options because oxyimino-cephalosporins are regularly prescribed, while carbapenems are considered last resort options in the treatment of multidrug resistant infections.[14−17]

The class D β-lactamases (DBLs) are the most diverse group among serine β-lactamases, with certain members possessing <20% sequence identity.[18,19] Despite their sequence diversity, DBLs have conserved structural features that are involved in the mechanism of hydrolysis. The mechanism of hydrolysis of β-lactam antibiotics by DBLs involves acylation and deacylation of the active-site serine and features a carboxylated lysine as the general base.[20,21] This reversible lysine modification, which is essential for DBL activity, is proposed to be a spontaneous reaction, facilitated by the hydrophobic environment of the active site and dependent on the protonation state of the lysine and the availability of CO_2.[17,20,22] Another property of DBLs that is not shared by other serine β-lactamases is inhibition by sodium chloride *in vitro*.[18] Most DBLs are fully inhibited at a sodium chloride concentration of 100 mM.[23] This property is

not fully understood, but a tyrosine residue, which is a constituent of a conserved YNG motif located in the vicinity of the DBL active site, has been implicated.[24] Héritier et al. showed that when the active-site tyrosine is substituted with phenylalanine, the resulting mutant is resistant to sodium chloride inhibition. Additionally, the mutant enzyme exhibited weaker activity for all the substrates tested.[24] A more recent study suggests that chloride competes with the carboxylation of the lysine and thereby inhibits DBLs by attenuating formation of the general base.[25]

DBLs are also called oxacillinases (or OXA-enzymes) on the basis of the properties of the first discovered members of this class, which have high catalytic efficiency for the hydrolysis of the semisynthetic penicillin oxacillin.[26] The rapid discovery of DBLs in recent years has led to the description of more than 400 OXA-enzymes.[27−30] On the basis of substrate specificity, they can be classified as narrow-spectrum oxacillinases, extended-spectrum β-lactamases (ESBLs), or carbapenem-hydrolyzing class D β-lactamases (CHDLs).[17,18,27,31] Furthermore, to better separate the OXA-enzymes, several subgroups have been formed on the basis of sequence homology. The enzymes within a subgroup differ from each other by one to five amino acids on average and generally have similar kinetic profiles.

OXA-48-like β-lactamases constitute a CHDL subgroup that is widespread in *K. pneumoniae* and other Enterobacteriaceae.[28,32] Their emergence represents an alarming development in carbapenem resistance worldwide. OXA-48, which was the first OXA-type carbapenemase isolated from enteric bacteria, has been identified for more than a decade from a multidrug resistant *K. pneumoniae* isolate, and it is the most widespread member of this subgroup.[28,33] It has a typical carbapenemase substrate profile with the highest catalytic efficiency for imipenem hydrolysis among all DBLs. However, its activity for oxyimino-cephalosporins is very modest and, in the case of ceftazidime, undetectable.[33,34] Currently, the OXA-48-like subgroup has 11 members, and they differ from OXA-48 by a few amino acid substitutions and deletions.[32] All of the OXA-48-like enzymes have substrate profiles similar to that of OXA-48 except for OXA-163.[32] The OXA-163 enzyme has a drastically reduced ability to hydrolyze carbapenems; however, unlike OXA-48, OXA-163 is able to hydrolyze the oxyimino-cephalosporin ceftazidime.[35]

OXA-163 is a relatively new β-lactamase that was identified in *K. pneumoniae* and *Enterobacter cloacae* from nosocomial infections.[35] OXA-163 differs from OXA-48 by an S212D substitution and a four-amino acid deletion (214-RIEP-217) (OXA-48 numbering).[34−36] The S212D substitution is located at the tip of the β5 strand, and the four-amino acid deletion is located in the loop region between the β5 and β6 strands.[34] The β5 strand forms one side of the active-site cavity and contains the conserved K(S/T)G motif (residues 208−210) typical for DBLs.[34] The loop between the β5 and β6 strands has been suggested to be important for the ability of an OXA variant to hydrolyze carbapenems, and therefore, the deletion may impact carbapenem hydrolysis.[34,37−39]

The goal of this study was to determine the structural basis for the change in substrate specificity observed in OXA-163 versus OXA-48. The crystal structure of OXA-163 determined at 1.72 Å resolution revealed that the four-amino acid deletion in OXA-163 expands the active-site pocket to accommodate the bulky side chain of ceftazidime, providing a molecular basis for the different substrate profiles of the two enzymes. Additionally, a second structure of OXA-163 was determined at 2.87 Å resolution using crystals from a different crystallization condition. This crystallization buffer contained iodide, which was found in the active site of the enzyme in the structure. Subsequent enzyme inhibition assays indicated that iodide is an inhibitor of both OXA-163 and OXA-48 as well as OXA-10, which is not in the OXA-48-like family. On the basis of the structural and inhibition analyses, it is proposed that halogen ions inhibit OXA-enzymes by changing the position of key active-site residues and inhibiting the formation of the carboxylated lysine, which is essential for the function of all OXA-enzymes.

MATERIALS AND METHODS

Cloning. The $bla_{OXA-163}$ gene containing the native signal sequence was inserted into the *Eco*RI site of the pET29a expression vector using T4 DNA ligase (New England Biolabs, Ipswich, MA). The bla_{OXA-48} gene in the pET29a plasmid was constructed by introducing the D212S substitution and 214-RIEP-217 insertion into the $bla_{OXA-163}$ gene by QuikChange polymerase chain reaction with *Pfu* Turbo DNA Polymerase (Agilent, Santa Clara, CA). The DNA sequence encoding the mature portion of bla_{OXA-10} was introduced into the pET28a vector using a Gibson assembly kit (New England Biolabs) with flanking *Nde*I and *Sac*I restriction sites that also contained an N-terminal His tag. DNA sequencing of the entire genes verified the sequences of $bla_{OXA-163}$, bla_{OXA-48}, and bla_{OXA-10}.

Protein Expression and Purification. OXA-48 and OXA-163 were expressed following a protocol previously described by Sosa-Peinado et al.[40] In brief, cells were grown in 1 L of LB broth containing 300 mM sorbitol, 2.5 mM betaine, and 30 μg/mL kanamycin to an OD_{600} of 0.6−0.8 before induction with 0.4 mM isopropyl β-D-1-thiogalactopyranoside (IPTG). The culture was then incubated at 23 °C for 20 h while being shaken. Afterward, the culture was centrifuged for 40 min at 7000*g*, and the supernatant was concentrated 10-fold using Vivaflow50 10MWCO (Sartorius, Goettingen, Germany) following dialysis (1:50) overnight at 4 °C against buffer containing 20 mM Tris and 0.4 M NaCl (pH 8.2). The proteins were purified to ∼95% homogeneity using a Fast Flow Chelating Sepharose (GE Healthcare, Pittsburgh, PA) packed in a column with a 16 mm diameter and a 170 mm bed length, loaded with zinc, and eluted with a linear gradient of 150 mM imidazole. Purity was determined by sodium dodecyl sulfate−polyacrylamide gel electrophoresis (SDS−PAGE), and protein fractions were concentrated with Vivaspin Turbo centrifugal filters 10MWCO (Sartorius). After concentration, size-exclusion chromatography using a HiLoad 16/600 Superdex 75 column (GE Healthcare) was performed in 10 mM Tris (pH 7.7) and 50 mM NaCl. Size-exclusion chromatography of both OXA-48 and OXA-163 indicated the presence of a dimer.[34] Fractions were concentrated, and the protein concentration was determined by absorbance measurements at 280 nm using an extinction coefficient of 63940 M^{-1} cm^{-1}.[41]

OXA-10 was expressed and purified as follows. LB medium (0.5 L) supplemented with 30 μg/mL kanamycin was inoculated with 10 mL of overnight culture of *Escherichia coli* BL21(DE3) carrying the pET28a-bla_{OXA-10} plasmid. Protein production was induced with 0.5 mM IPTG when the cell culture reached an OD_{600} of 0.8. The culture was then incubated at 30 °C for 20 h. Afterward, the culture was centrifuged for 40 min at 7000*g*. The cell pellet was resuspended in 20 mL of lysis buffer containing 50 mM

phosphate (pH 7.4), 40 μM $MgCl_2$, and 10 ng/mL DNase. Cell contents were released using a French press, and the lysate was centrifuged at 10000*g* for 30 min. The supernatant was passed through a HisTrap FF column (GE Healthcare), and the protein was eluted with a linear gradient of 500 mM imidazole. Protein was concentrated by buffer exchange using Vivaspin Turbo centrifugal filters 10MWCO (Sartorius). Protein purity was determined by SDS−PAGE. The protein concentration was determined by absorbance measurements at 280 nm using an extinction coefficient of 47565 M^{-1} cm^{-1}. The N-terminal His tag was not removed because steady-state kinetics of the His-OXA-10 enzyme confirmed that activity is not affected by the tag (data not shown).

Enzyme Kinetic Studies. Assays were performed on a DU800 spectrophotometer at 30 °C in 50 mM sodium phosphate buffer (pH 7.2) supplemented with 15 mM sodium bicarbonate as previously described.[42] Substrate hydrolysis was followed at wavelengths of 260 nm for ceftazidime ($\Delta\varepsilon$ = −6900 M^{-1} cm^{-1}) and cefotaxime ($\Delta\varepsilon$ = −7500 M^{-1} cm^{-1}), 262 nm for cephalothin ($\Delta\varepsilon$ = −7660 M^{-1} cm^{-1}), 298 nm for meropenem ($\Delta\varepsilon$ = −7200 M^{-1} cm^{-1}), and 299 nm for imipenem ($\Delta\varepsilon$ = −9670 M^{-1} cm^{-1}), doripenem ($\Delta\varepsilon$ = −11540 M^{-1} cm^{-1}), and nitrocefin ($\Delta\varepsilon$ = 20500 M^{-1} cm^{-1}). Enzyme kinetic data was analyzed with GraphPad Prism 6 (GraphPad Software, Inc., La Jolla, CA) and fitted to the Michaelis−Menten equation. In the cases in which V_{max} could not be reached because of a high K_m value, the catalytic efficiency (k_{cat}/K_m) was calculated by fitting the data to a first-order kinetics equation.[43] Inhibition by halogen ions was examined with NaI, NaBr, NaCl, or NaF using cephalothin (50 μM for OXA-48 and 12 μM for OXA-10) and 13 μM cefotaxime (OXA-163) as substrates in 50 mM sodium phosphate buffer (pH 7.2). The enzymes were preincubated with increasing concentrations of inhibitor for 30 min at room temperature and for an additional 10 min at 30 °C before hydrolysis was monitored. The concentration that reduced the level of hydrolysis by 50% (IC_{50}) was determined.[44]

Crystallization and Data Collection. Crystal conditions were screened with 10 mg/mL concentrated protein using a range of commercially available screens. OXA-163 crystals grew in 0.1 M HEPES (pH 7.7) and 14% (w/v) PEG 8000. Crystals were cryoprotected with the well solution containing 20% (v/v) PEG 600 and flash-frozen in liquid nitrogen. A 1.72 Å resolution data set was collected on beamline 5.0.1 of the Berkeley Center for Structural Biology in the context of the Collaborative Crystallography Program. Another crystallization condition was identified containing 0.2 M NaI (pH 5.5) and 15% PEG 3350. Crystals were cryoprotected with the well solution containing 30% glycerol. A 2.87 Å data set was collected at the Baylor College of Medicine on a Rigaku FR-E SuperBright High-Brilliance Rotating Anode Generator.

Structure Determination and Refinement. Diffraction data were processed using the CCP4i suite.[45] iMOSFLM was used to process and integrate the images.[46] The crystal structures were determined by molecular replacement using OXA-48 [Protein Data Bank (PDB) entry 3HBR] as the phasing model with MOLREP.[47] After one round of REFMAC5 refinement, AutoBuild was used (Phenix suite) followed by manual inspection with COOT.[48−50] Several cycles of refinement were performed using phenix.refine (native) and REFMAC5 (with iodide).[51,52] The presence of iodide was confirmed by computing the anomalous difference map using the data set without averaging the Friedel pair intensities (R_{meas} = 13.3%). Data collection and refinement statistics are listed in Table 1.

Table 1. Data Collection and Refinement Statistics

	OXA-163 (PDB entry 4S2L)	OXA-163 (PDB entry 4S2M)
	Data Collection	
wavelength (Å)	0.997	1.54
resolution range (Å)	38.2−1.72 (1.78−1.72)	61.77−2.87 (2.98−2.87)
space group	$P2_1$	$P1$
unit cell dimensions		
a, *b*, *c* (Å)	44.9, 125.8, 49.7	67.6, 68.4, 70.2
α, β, γ (deg)	90.0, 116.8, 90.0	62.2, 68.0, 71.6
no. of unique reflections	51864 (5184)	22060 (2111)
multiplicity	10.4 (10.3)	8.2 (7.9)
completeness (%)	99.7 (99.8)	95.0 (90.3)
mean $I/\sigma(I)$	52.5 (3.40)	5.1 (2.0)
Wilson *B* factor (Å^2)	18.3	58.8
R_{merge} (%)	7.7 (53)	9.3 (32.5)
	Refinement	
R_{work} (R_{free}) (%)	19.5 (23.7)	20.1 (25.6)
no. of non-hydrogen atoms	4642	7752
protein	3883	7661
ligands		20
waters	759	71
no. of protein residues	474	935
root-mean-square deviation for bond lengths (Å)	0.009	0.013
root-mean-square deviation for bond angles (deg)	1.18	1.49
Ramachandran		
favored (%)	95	96
outliers (%)	0	0.33
average *B* factor (Å^2)	22.9	55.5
protein	21	55.6
ligands	–	80.9
waters	32.8	30.4

Molecular Docking. Docking experiments were performed with cefotaxime (PDB ligand id CE3) and ceftazidime. Ceftazidime (CID481173) coordinates were retrieved from the PubChem compound database.[53] The substrate molecule was docked into the crystal structure of OXA-48 (PDB entry 3HBR) and OXA-163 (PDB entry 4S2L) using AutoDock Vina (The Scripps Institute, La Jolla, CA).[54] Before being docked, the proteins were processed by adding polar hydrogen atoms using AutoDockTools. The Lamarckian genetic algorithm was used to generate possible protein−ligand binding conformations.[55] The receptor (β-lactamase) was treated as a rigid body, with all possible rotational angles in the substrate. The grid box was centered on the Ser70 residue with the size (22 Å × 24 Å ×

Table 2. Steady-State Kinetic Parameters of OXA-48 and OXA-163 for Cephalosporin and Carbapenem Substrates

	OXA-48			OXA-163		
substrate	k_{cat} (s^{-1})	K_m (μM)	k_{cat}/K_m (s^{-1} M^{-1})	k_{cat} (s^{-1})	K_m (μM)	k_{cat}/K_m (s^{-1} M^{-1})
nitrocefin	143 ± 24	36 ± 7	4.0×10^6	34 ± 2	19 ± 8	1.8×10^6
cephalothin	2.8 ± 0.1	140 ± 10	2.0×10^4	1.7 ± 0.1	3.4 ± 0.4	5.0×10^5
cefotaxime	NM[a]	>1000	4.7×10^3	14 ± 1	36 ± 11	3.8×10^5
ceftazidime	ND[b]	–	–	NM	>1000	300
imipenem	2.7 ± 0.2	3.7 ± 0.7	9.0×10^5	0.004 ± 0.001	3.6 ± 1.0	1.1×10^3
meropenem	0.11 ± 0.01	6.0 ± 1.2	1.7×10^4	0.021 ± 0.001	5.3 ± 0.5	4.0×10^3
doripenem	0.066 ± 0.002	4.1 ± 0.6	1.6×10^4	0.018 ± 0.001	5.0 ± 0.4	3.6×10^3

[a]Not measurable. It was not possible to measure V_{max} because of the high K_m value. [b]Not detected. No detectable hydrolysis with up to 5 μM enzyme and 500 μM substrate.

24 Å) of the box adjusted to cover the entire catalytic site. Docking was conducted with an exhaustiveness of 8.

PDB Accession Codes and Programs Used. The atomic coordinates of the OXA-163 structure were deposited in the Protein Data Bank[56] as entries 4S2L (native) and 4S2M (with iodide). Alignment and root-mean-square deviation (rmsd) calculations were performed by the SSM procedure using COOT.[57] All structural figures were generated with UCSF Chimera.[58]

RESULTS AND DISCUSSION

Enzyme Kinetic Parameters of OXA-48 and OXA-163 for Cephalosporins and Carbapenems. To examine if the changes in sequence result in different substrate specificity between OXA-48 and OXA-163, steady-state kinetic parameters were determined for several clinically used cephalosporin and carbapenem substrates as well as the colorimetric cephalosporin, nitrocefin. For OXA-48, the highest catalytic efficiency is observed for nitrocefin hydrolysis (4.0×10^6 s^{-1} M^{-1}) (Table 2). With regard to clinically relevant substrates, however, the results confirm that OXA-48 has a preference for carbapenems, with the highest catalytic efficiency (k_{cat}/K_m) observed for imipenem hydrolysis (9.0×10^5 s^{-1} M^{-1}).[33,34] Compared to imipenem, the OXA-48 k_{cat}/K_m value is 53-fold smaller for meropenem and 56-fold smaller for doripenem hydrolysis because of a reduction in the turnover number (k_{cat}). In addition, the early cephalosporin, cephalothin, is hydrolyzed with a k_{cat}/K_m slightly higher than that of the oxyimino-cephalosporin cefotaxime mainly because of a lower K_m value. Finally, the steady-state kinetic analysis indicates OXA-48 does not hydrolyze the bulky oxyimino-cephalosporin ceftazidime.[33,59]

The substrate profile of OXA-163 is substantially different from that of OXA-48. Unlike OXA-48, OXA-163 has a preference for cephalosporin substrates (Table 2). The highest k_{cat}/K_m values were observed for nitrocefin (1.8×10^6 s^{-1} M^{-1}), cephalothin (5.0×10^5 s^{-1} M^{-1}), and cefotaxime (3.8×10^5 s^{-1} M^{-1}). Ceftazidime was hydrolyzed with the lowest k_{cat}/K_m (300 s^{-1} M^{-1}) among the cephalosporins tested because of a high K_m value. Nevertheless, OXA-163 does hydrolyze ceftazidime. The carbapenemase activity of OXA-163 is attenuated largely because of a reduction in the turnover number, while the affinity is very similar to the affinity of OXA-48 for carbapenems. This leads to a decrease of 820-fold in the catalytic efficiency of OXA-163 for imipenem in comparison to that of OXA-48. However, it is noteworthy that the catalytic efficiencies of OXA-163 are higher for meropenem and doripenem than for imipenem, which is the opposite of that observed for OXA-48. This change in order of preference is due to a larger reduction in k_{cat} for imipenem hydrolysis compared to those of meropenem and doripenem in the OXA-163 enzyme (Table 2). Although the reason for this cannot be known without further structural data, it is possible that the smaller size of imipenem in comparison to meropenem and doripenem allows it to fit better in the active site of OXA-48, leading to a higher rate of turnover of imipenem by OXA-48, which is then lost due to the active-site expansion that occurs in OXA-163 as described below.

In summary, the results confirm the ability of the OXA-48 active site to accommodate carbapenem substrates, particularly imipenem, while it is unable to hydrolyze ceftazidime, a bulkier oxyimino-cephalosporin.[34,35] When OXA-48 is transformed to OXA-163 by mutations, it loses its high catalytic efficiency for carbapenems, particularly imipenem, but gains the ability to hydrolyze ceftazidime. Therefore, the 214-RIEP-217 deletion and S212D substitution alter the substrate specificity of the enzyme. This finding is consistent with previously published kinetic data showing a significant increase in the level of ceftazidime hydrolysis compared to that of OXA-48.[34,35] Additionally, two other members of the OXA-48-like β-lactamases, OXA-247[60] and OXA-405, which differ from OXA-48 by a four-amino acid deletion, 214-RIEP-218 and 213-TRIE-217, respectively, have significantly lowered activity toward carbapenem substrates compared to that of OXA-48 (P. Nordmann, personal communication).

1.72 Å Crystal Structure of OXA-163. The four-amino acid deletion and S212D substitution transform OXA-48 into OXA-163 and change the substrate profile of the enzyme. To investigate the structural basis for the changes in specificity, the X-ray crystal structure of OXA-163 was determined. The asymmetric unit in the crystal consists of one dimer with the same space group ($P2_1$) as the previously published crystal structure of OXA-48.[34] The mature OXA-163 enzyme consists of 237 residues and has a two-domain fold typical of DBLs with a globular α-domain and an α/β-domain with the active site located between the two domains (Figure 1A). The active site of OXA-163 forms a groove in the protein surface between the two domains. The clefts of the groove are formed on one side by the β5 strand and the N-terminus of helix α11, and on the other by helices α5 and α6 and the Ω-loop (Figure 1A). The three conserved motifs characteristic of the active site of DBLs are outlined in Figure 1A. Motif I consists of the catalytic Ser70 as well as Thr71, Phe72, and carboxylated Lys73. The carboxylate moiety attached to εN shows clear density (Figure 1B) in both monomers. Motif II contains residues Ser118, Val119, and Val120 and is located on the loop between the α5 and α6 helices, while motif III consists of β5 strand residues Lys208, Thr209, and Gly210. Lys208 interacts with Ser118

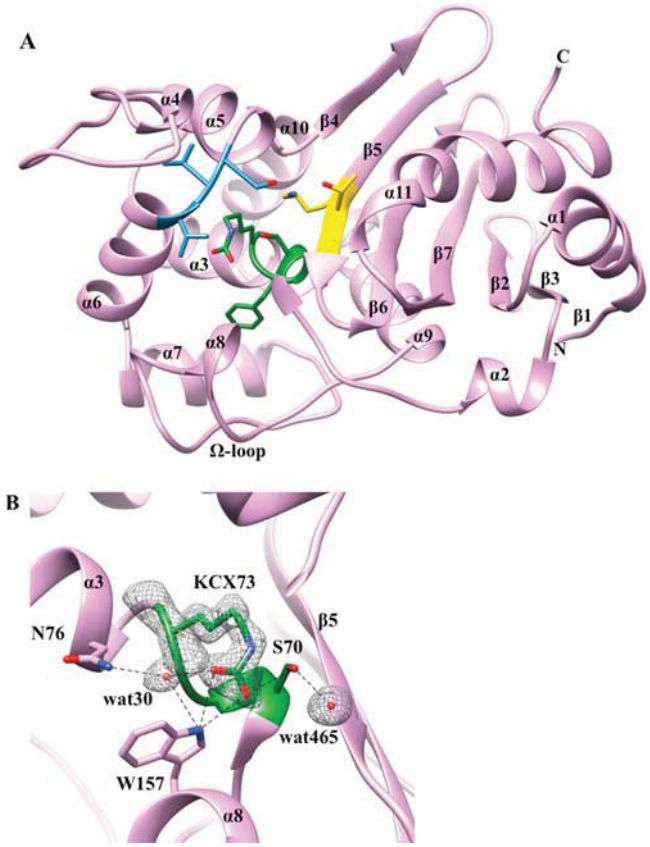

Figure 1. Crystal structure of OXA-163. (A) Ribbon representation of OXA-163 with secondary structural elements labeled. The three conserved DBL motifs are shown with their respective residues as a stick model: motif I in green (Ser70, Thr71, Phe72, and Lys73), motif II in blue (Ser118, Val119, and Val120), and motif III in yellow (Lys208, Thr209, and Gly210). (B) Active-site region of OXA-163. The carboxylated side chain of the active-site residue Lys73 is shown together with nearby interacting residues and water molecules. Superimposed is the $2F_o - F_c$ simulated annealing difference map calculated with phases from the final refined model and contoured at the 2.5σ level. The carboxylate moiety is coordinated by Ser70, Trp157, and, via a water molecule, Asn76. Red spheres represent the two water molecules.

from motif II, and these residues have been suggested to play a role in substrate binding and proton transfer in the acylation reaction in DBLs.[23] Overall, the OXA-163 structure is quite similar to the OXA-48 structure[34] (Figure 2A) with an rmsd of 0.271 Å for the matching Cα atoms. However, the $\beta5-\beta6$ loop is shorter because of the 214-RIEP-217 deletion that results in an expanded active-site cavity compared to that of OXA-48. Like that of OXA-48, the quaternary structure of OXA-163 is dimeric, which is not surprising because the residues at the dimerization surface are identical.

A comparison of the active sites of OXA-48 and OXA-163 reveals several differences. (i) In OXA-48, the side chain of Arg214 creates one side of the active site by forming an electrostatic interaction with Asp159 positioned on the Ω-loop (Figure 2A). In OXA-163, Arg214 is within the four-amino acid deletion, which eliminates one boundary of the active site and elongates the groove (Figure 2A). Arg214 has been suggested to form electrostatic interactions with carbapenem substrates that facilitate hydrolysis. This could explain the low activity of OXA-163 toward carbapenems.[34] Additionally, this expansion of the active site of OXA-163 is consistent with the ability of the enzyme to accommodate a larger substrate such as ceftazidime. The hypothesis that Arg214 contributes to the inability of OXA-48 to accommodate ceftazidime is also supported by the observation that a shorter and uncharged side chain at position 214 (R to S) results in an increase in ceftazidime hydrolysis activity by OXA-232 (an OXA-48-like enzyme).[32] (ii) The 214-RIEP-217 deletion shortens and alters the conformation of the $\beta5-\beta6$ loop in OXA-163 compared to that in OXA-48 (Figure 2A). The position and length of this loop have also been associated with efficient deacylation in carbapenem hydrolysis.[34,39] The altered size and position of the $\beta5-\beta6$ loop in OXA-163 may contribute to the reduced level of hydrolysis of carbapenems by this enzyme (Table 2). At the same time, this structural change widens the active site of OXA-163 and provides extra space for the oxyimino group of ceftazidime. (iii) The 214-RIEP-217 deletion also causes displacement of Thr213, which in part contributes to the enlargement of the active-site cavity of OXA-163. The backbone, together with the side chain of Thr213, adopts a different conformation and moves away from the active site (~4 Å), creating a shorter $\beta5-\beta6$ loop (Figure 2A,B). Lys218, which is now adjacent to Thr213, is also displaced farther from the active site (5 Å). (iv) The newly introduced aspartate at position 212 is also likely to contribute to the changes in OXA-163 specificity. Compared to Ser212 in OXA-48, the Asp side chain is pointed toward the $\beta6$ strand to form hydrogen bonds with the -NH main-chain groups of Lys218 and Ile219 (Figure 2B). This draws the $\beta5$ strand main chain closer to the $\beta6$ strand and widens the active-site wall formed by the $\beta5$ strand. (v) Finally, several water molecules that are part of a larger interaction network that includes Ser70, Ser118, Thr209, Tyr211, Thr213, and Arg250 in OXA-48 are misplaced or missing in the OXA-163 structure (Figure 2C). This interacting network in OXA-48 was suggested previously to be important in the efficiency of the deacylation reaction for carbapenems.[34] This observation is consistent with the large decrease in the turnover number of OXA-163 for carbapenems (Table 2).

In summary, several spatial modifications in the active site of OXA-163 ultimately expand the active site and rearrange the inter-residue interaction network. The larger active site is consistent with improved accommodation of ceftazidime and the loss of critical interactions with carbapenem substrates, resulting in an altered substrate profile for OXA-163.

Crystal Structure of OXA-163 in the Presence of Iodide. As described above, a second structure of OXA-163 was determined at 2.87 Å from crystals formed under a condition that included 200 mM sodium iodide. The observed asymmetric unit consists of four protein molecules (two dimers) in a *P*1 space group. The dimer interface of the structure with iodide is unchanged compared to that of native OXA-163 and OXA-48 structures. The 2.87 Å resolution of the structure with iodide clearly reveals the electron density of the main-chain backbone. An exception was part of the loop (residues 244–247) connecting the $\beta7$ strand and α-helix $\alpha11$, which did not show density and was not modeled in the final structure. Some of the solvent-exposed side chains, particularly lysines and glutamates, were also not visualized. However, the electron density for the active-site lysine 73, which acts as the general base in its carboxylated form,[20] was clearly resolved and did not show an extension of the side chain, indicating the carboxylate group was absent. Instead, an iodide ion was observed in all four molecules in the asymmetric unit at the

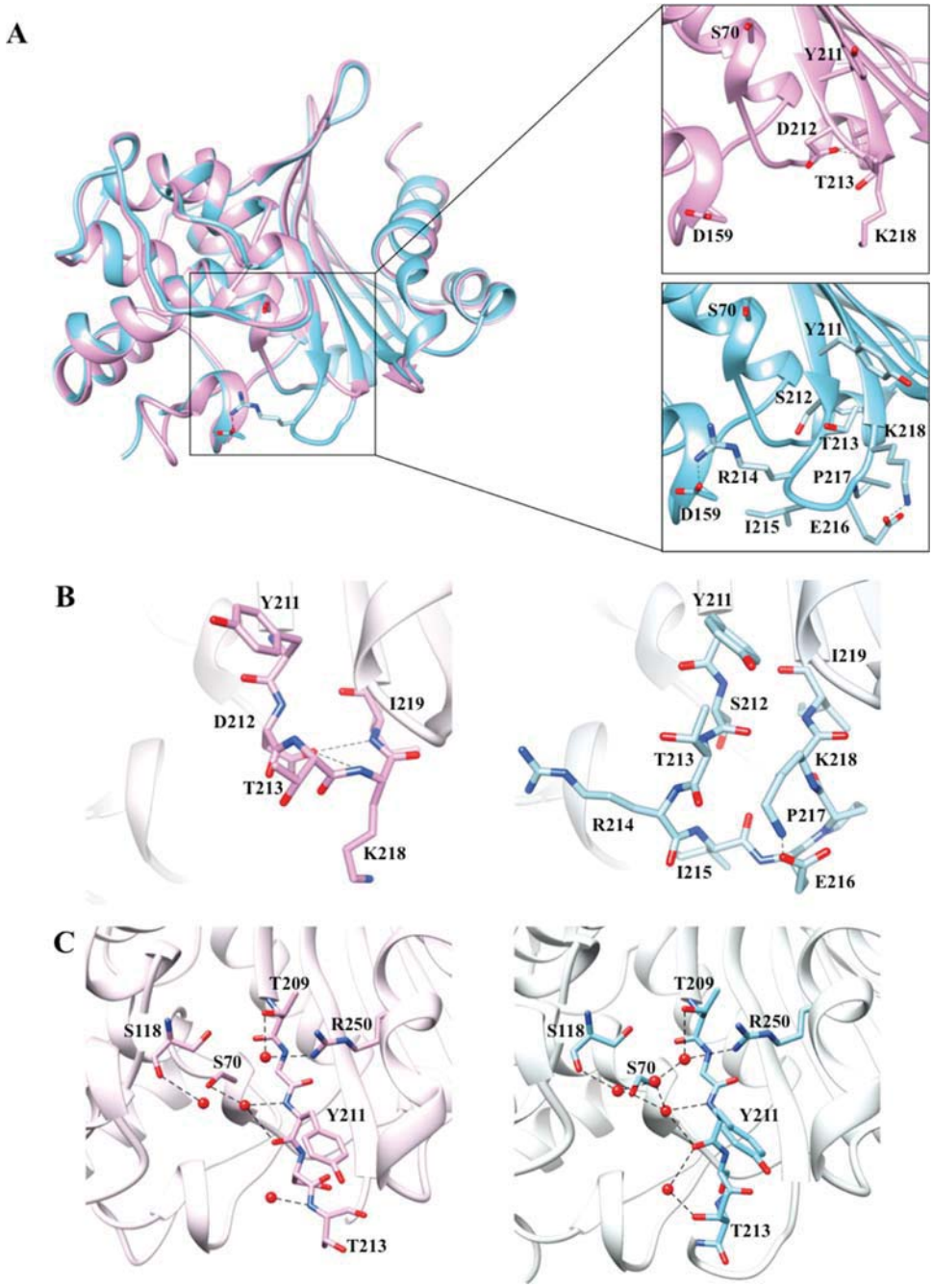

Figure 2. Comparison of the tertiary structures of OXA-48 at 1.9 Å and OXA-163 at 1.72-Å resolution. (A) Cα alignment of OXA-48 (blue) and OXA-163 (lavender). The insets provide a detailed view of the β5−β6 loop region residues represented as a stick model with black dashes representing interactions. Arg214 in OXA-48 forms an electrostatic interaction with Asp159 located on the Ω-loop. This interaction confines the bottom boundary of the active-site cavity in OXA-48. In OXA-163, Arg214 is absent so the interaction is lost, resulting in an expanded active-site cavity. (B) Stick representation of the β5−β6 loop region of OXA-48 and OXA-163. The OXA-163 residues that undergo the largest movement compared to those of residues of OXA-48 are Tyr211, Thr213, and Lys218. The S212D substitution results in newly formed hydrogen bonds between the Asp212 side chain and the -NH main chain of Lys218 and Ile219 represented as black dashed lines. (C) Active-site hydrogen bond network in OXA-48 and OXA-163. Several water molecules exhibit altered positions or are missing in OXA-163 compared to OXA-48. Distances of 2.5−3.8 Å are shown as dashed black lines.

location where the εN-carboxylate has been observed in other crystal structures. Previously, a chloride ion has been observed at this location in the crystal structures of wild-type OXA-10 and its V117T mutant.[23,25]

The two OXA-163 structures determined here are very similar with an rmsd of 0.425 Å for their main-chain Cα atoms (Figure 3A). However, the presence of iodide causes a series of rearrangements in the active site, which ultimately leads to distortion of the β5 strand and occlusion of the active-site serine (Figure 3A). In the presence of iodide, Lys73 is not carboxylated and adopts a conformation in which its side chain points away from the active site and the bound iodide. Similarly, the side chain of Lys208 is also dramatically shifted, pointing away from the active site. In fact, Nζ of Lys73 in the

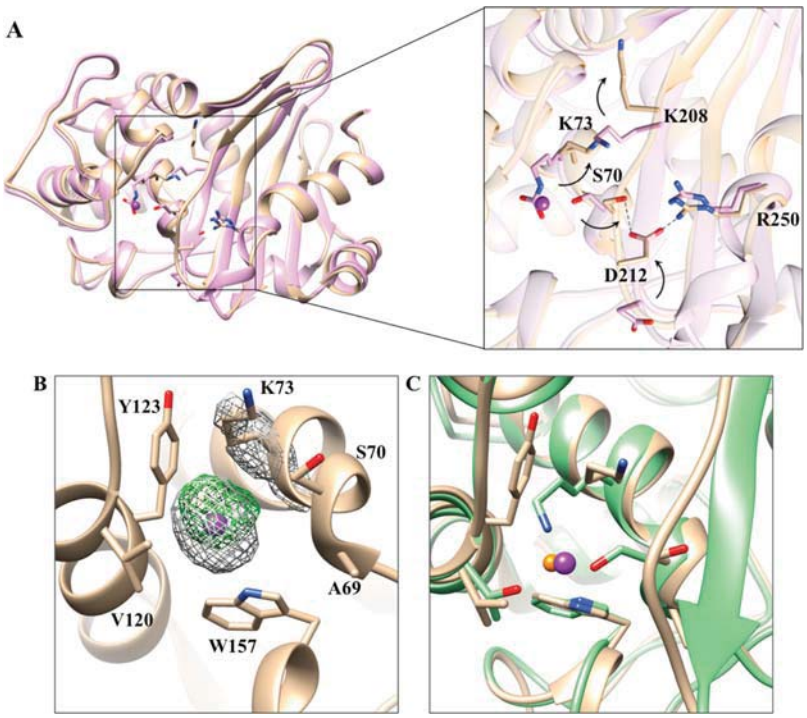

Figure 3. Alignment of the two OXA-163 structures and comparison of chloride and iodide ions in the active site of class D enzymes. (A) 1.72 Å structure (lavender) and 2.87 Å structure with iodide (tan). Iodide is represented as a dark purple sphere with an arbitrary radius. The inset provides a more detailed view of the residues (stick model) that undergo large conformational changes due to the presence of the iodide in the active site. In the iodide structure, Asp212 exhibits an altered conformation that results in the formation of an electrostatic interaction with Arg250 (black dashed line). Additionally, the Asp212 residue is within hydrogen bonding distance of the catalytic Ser70. The arrows represent the direction of the rearrangements that occur in the iodide structure. (B) Iodide and its surrounding environment in the active site. In gray mesh, superimposed, is the $2F_o - F_c$ simulated annealing difference map calculated with phases from the final refined model and contoured at the 3.0σ level. In green mesh is the anomalous difference map contoured at 5σ. Residues surrounding iodide are labeled and shown as stick models. (C) Overlay of OXA-10 (green) inhibited by chloride (orange sphere) and OXA-163 (tan) inhibited by iodide (purple sphere). Iodide is larger than chloride and results in structural rearrangements of the surrounding residues.

OXA-163 iodide-bound structure occupies the position where Nζ of Lys208 is found in the OXA-163 structure without iodide and in OXA-48 (Figure 3A). Another major change observed in the iodide-bound structure is with respect to Asp212, at the tip of the β5 strand, which moves 5 Å toward the active site where it hydrogen bonds with Ser70 and engages in electrostatic interactions with Arg250 (Figure 3A). These rearrangements of Lys73, Lys208, and Asp212 along with the newly formed network of interactions involving Ser70, Asp212, and Arg250 result in the occlusion of the active site. Previous structural studies of DBLs showed that Arg250 plays an important role in binding and positioning of the carbapenem in the active site of the enzyme.[34,37,61] The rearrangements in the iodide-bound structure result in a short β5 strand (three residues, 204−206), which interacts with only the β4 strand. This is in contrast to the OXA-163 structure without iodide, in which the β5 strand is nine residues long (204−212), forming an antiparallel β-sheet involving strands β4 and β6.

The iodide ion found in the active site of OXA-163 is located in a hydrophobic pocket (Figure 3B). It is surrounded mainly by nonpolar and aromatic moieties, with the exception of the polar interaction with εNH of Trp157 (3.7 Å). The hydrophobic interactions include the side-chain hydrocarbons of Lys73 (3.8 Å), the aromatic component of Tyr123 (4.3 Å), the side chain of Val120 (4.5 Å), the aromatic component of Trp157 (4.5 Å), and the main-chain hydrocarbons of Ser70 (4.3 Å) and Ala69 (4.7 Å). The types of displacements observed in the OXA-163 structure with iodide, including alternative side-chain conformations and main-chain movements, have been observed in several crystal structures that accommodate an iodide ion in the proximity of a hydrophobic region.[62]

Iodide ions have not previously been observed in the active sites of OXA-enzyme crystal structures. However, chloride ions have been identified in the active site of OXA-10.[23,25] The position of the chloride ion in the OXA-10 V117T mutant is very similar to the iodide ion in the OXA-163 structure (Figure 3C). However, the iodide occupies a larger volume and results in additional structural displacements in the active site compared to those with chloride. Also, the interactions of the chloride ion with OXA-10 are exclusively electrostatic, while the iodide interactions are overwhelmingly hydrophobic. This is possibly due to the difference in size between the two ion species and their different ability to tolerate a hydrophobic environment. Chloride is smaller and can replace the carboxylate group that is attached to Lys73 and thereby maintain electrostatic interactions with the surrounding residues. On the other hand, iodide is larger and cannot be accommodated in the same location as the carboxylate without expanding the cavity and rearranging the side chains of the nearby residues. Additionally, iodide ions are more tolerant of a hydrophobic environment than chloride ions and are found in hydrophobic patches of proteins.[62−64] Tyr141 from the YGN conserved motif that has been implicated in chloride inhibition of OXA-enzymes is 10 Å from the iodide in OXA-163, suggesting it has a minimal role in the binding of the iodide.[24]

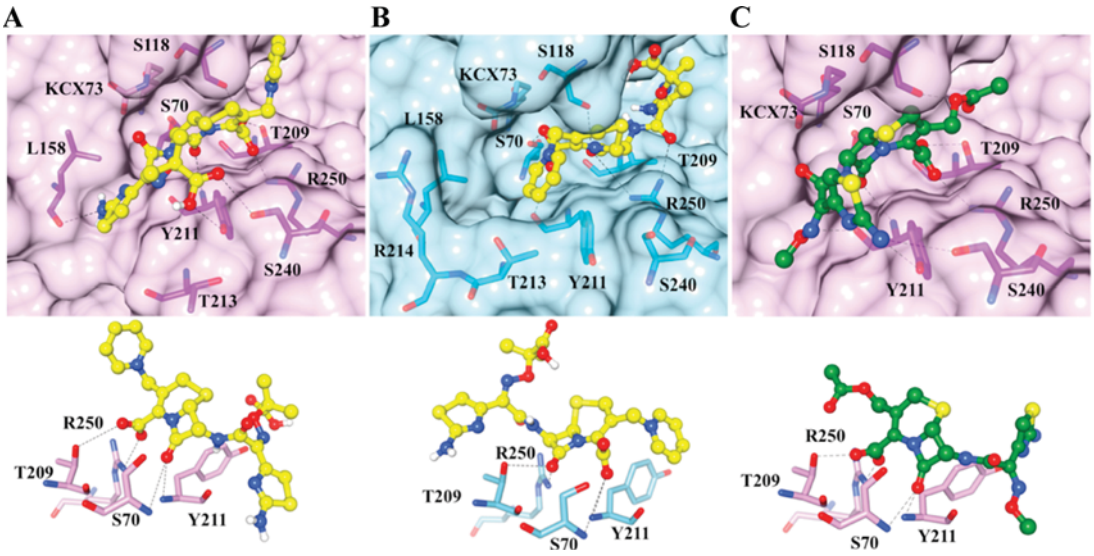

Figure 4. Docking results of ceftazidime with OXA-163 (lavender) and OXA-48 (light blue) and cefotaxime with OXA-163. The protein structures are shown in surface representation, and the residues that interact with ceftazidime and cefotaxime are labeled and shown as sticks. Ceftazidime and cefotaxime are shown as yellow and green sticks, respectively. The carboxylated Lys73, which is not within interaction distance of the substrate, is also shown and is labeled KCX73. Black dashed lines represent hydrogen bonds. The top part of panel A shows the conformation with the lowest binding energy of ceftazidime for OXA-163. The top part of panel B shows the conformation of ceftazidime with the lowest binding energy for OXA-48. In OXA-48, the ceftazidime molecule is flipped compared to the conformation in OXA-163. The docked conformation of ceftazidime in the active site of OXA-48 is not consistent with catalysis. The top part of panel C shows the conformation with the lowest binding energy for OXA-163 with cefotaxime. The bottom parts show the oxyanion hole formed by Ser70 and Tyr211 and the interaction between the carboxylate group of ceftazidime or ceftotaxime and Thr209 and Arg250. These interactions are altered in the docked conformation of ceftazidime in OXA-48 (panel B, bottom) such that the β-lactam carbonyl interacts with Thr209 and Arg250 while Ser70 and Tyr211 interact with the carboxylate moiety.

Docking of Ceftazidime into the Active Sites of OXA-48 and OXA-163. To further investigate why ceftazidime is hydrolyzed by OXA-163 but not OXA-48, molecular docking of ceftazidime was performed using Autodock Vena.[54] The protein structures used for docking were OXA-48 (PDB entry 3HBR)[34] and the OXA-163 structure without iodide (PDB entry 4S2L). The same constraints were used for both proteins (Materials and Methods). Each docking round gave nine possible conformations, ranked from highest to lowest predicted affinity. It should be noted that all nine conformations of ceftazidime in OXA-48 had the oxyimino side chain of ceftazidime pointed toward Lys208 and the top of the active site (Figure 4B). The hydrolysis of ceftazidime is not mechanistically feasible from this conformation because the β-lactam carbonyl oxygen is not in the proximity of the NH main-chain atoms of Ser70 (5.3 Å) and Tyr211 (4.2 Å), which form the oxyanion hole in DBLs. Also, the position of the carboxylate group of ceftazidime does not form electrostatic interactions with Thr209 and Arg250. These residues have been identified previously to form strong electrostatic interactions with the substrate carboxylate in crystal structures of OXA-enzymes.[61,65] The dominance of this catalytically nonproductive conformation of ceftazidime in the docking results is due to the narrow active-site cavity of OXA-48 that is confined at the bottom by Arg214 and the longer $\beta5-\beta6$ loop and Thr213. The narrow cavity sterically hinders the formation of a more productive conformation of the oxyimino side chain of ceftazidime.

In contrast, the highest-affinity binding conformation predicted for ceftazidime bound to OXA-163 has the substrate in an orientation where the oxyimino side chain occupies the bottom portion of the active-site cavity (Figure 4A). Importantly, the carbonyl oxygen of the β-lactam ring of ceftazidime is hydrogen-bonded to the main-chain nitrogens of Ser70 and Tyr211 to form the oxyanion hole so that the substrate is in a catalytically competent conformation. The carboxylated Lys73 is on the other side of Ser70 and is not within an interaction distance of the substrate. In addition, the carboxylic acid moiety of the oxyimino group is within hydrogen bonding distance of Oη of tyrosine 211 and Oγ of serine 240. These interactions turn the imino-thiazole ring toward the Ω-loop where it interacts with the main-chain CO of leucine 158. This flip in the conformation of ceftazidime in the active site of OXA-163, compared to the conformation in OXA-48, is allowed by the expanded cavity resulting from the absence of the Arg214 side chain and the shorter $\beta5-\beta6$ loop. The inability of ceftazidime to be docked in the active site of OXA-48 in an orientation that is catalytically feasible is consistent with the hypothesis that the active-site cavity of OXA-48 is too small to fit the bulky ceftazidime substrate.

OXA-163 also exhibits an increased k_{cat}/K_m for hydrolysis of the oxyimino-cephalosporin cefotaxime compared to that of the OXA-48 enzyme (Table 2). This is due to a large decrease in K_m from >1000 μM for OXA-48 to 36 μM for OXA-163. The K_m of cefotaxime for OXA-163 is also much lower than that observed for ceftazidime. Molecular docking was therefore performed with OXA-163 with cefotaxime for comparison with the ceftazidime docking results. The docking results show that cefotaxime fits in the active site in a catalytically productive pose with the β-lactam carbonyl oxygen present in the oxyanion hole as observed for ceftazidime (Figure 4C). However, cefotaxime is embedded deeper in the active-site cavity and also has the aminothiazole ring flipped 180° pointing toward the solvent compared to ceftazidime. Although there is no X-ray structural information available to examine the molecular details of OXA-163 binding with cefotaxime and ceftazidime, the docking studies suggest cefotaxime can assume a more

buried position in the active site, which may explain the lower K_m observed for cefotaxime hydrolysis by OXA-163 (Table 2).

Halogen Ion Inhibition of OXA-enzymes. The observation of an iodide ion and the associated rearrangement of key active-site residues as well as the absence of carboxylated Lys73 in the crystal structure of OXA-163 in the presence of iodide suggest that iodide ions inhibit the activity of the enzyme. Considering the relative ability of iodide versus the other halogens to enter a hydrophobic hydration shell[66] and the hydrophobic environment of the active site of DBLs, we predict that iodide would be the most potent inhibitor among halogen ions. To test these ideas, OXA-48 and OXA-163 were examined for halogen ion inhibition. The substrates cephalothin (OXA-48) and cefotaxime (OXA-163) were used to measure the activity of the enzymes in the presence of halogen ions. It was found that halogen ions inhibit both OXA-48 and OXA-163 with similar potencies (Table 3). The IC_{50} depends on the size

Table 3. IC_{50} Values of OXA-48, OXA-163, and OXA-10 for Halogen Ions

	IC_{50} (mM)[a]		
halide	OXA-48	OXA-163	OXA-10
NaF	207 ± 11	216 ± 20	264 ± 20
NaCl	109 ± 12	97 ± 13	67 ± 10
NaBr	35 ± 7	29 ± 9	27 ± 6
NaI	14 ± 5	10 ± 4	4 ± 2

[a]Values and standard deviations were determined from three separate experiments.

of the ion, the larger ions being better inhibitors. The crystal structure of OXA-163 with iodide in the active site shows that iodide is not within hydrogen bond distance of any of the active-site residues except the εNH atom of Trp157 (Figure 3B). The inhibition assay results are consistent with the ability of the halide ion to be accommodated in a hydrophobic environment because the polar nature of the halogens decreases with increasing size.[67]

To test whether halogens inhibit other class D enzymes that are not members of the OXA-48-like family, inhibition assays were performed with OXA-10 β-lactamase (Table 3). OXA-10 has been studied extensively, and it was the first class D β-lactamase with a determined X-ray structure.[23] The sequence of OXA-10 is 46% identical with that of OXA-48 and it is a narrow-spectrum β-lactamase with high catalytic efficiency for penicillins and early cephalosporins.[33,39] As indicated in Table 3, the activity of OXA-10 is inhibited by halogens with a potency similar to and on the same order of magnitude as those of OXA-48 and OXA-163 where larger ions are better inhibitors. Additionally, the iodide IC_{50} for OXA-10 is 4.2 mM, which is approximately 2.5-fold more potent than those of both OXA-48 and OXA-163.

Taken together, the inhibition studies suggest that halogen inhibition might be a property of all class D β-lactamases. Although the IC_{50} values are in low millimolar range (for iodide), the inhibition of carboxylation of Lys73 by halogens may provide a starting point in the development of new β-lactamase inhibitors given the fact that carboxylation of the active-site lysine is an absolute requirement for the function of all class D β-lactamases.

CONCLUSIONS

As multidrug resistant infections are on the rise, carbapenems represent one of the last-resort antibiotics for the treatment of these infections.[16] Carbapenem-hydrolyzing class D β-lactamases (CHDLs) inactivate carbapenems and confer resistance to these drugs. One common CHDL that is widespread in clinics is OXA-48.[28,33] OXA-163 is a variant of OXA-48 with attenuated catalytic efficiency for carbapenems that has gained the ability to hydrolyze ceftazidime, expanding the ability of this class of enzymes to hydrolyze β-lactams.[32,35] Our structural data suggest that in OXA-163 an enlargement of the active-site cavity that allows this enzyme to accommodate ceftazidime occurs. The enlargement of the active site provides a molecular basis for the distinct substrate profile of these two closely related enzymes and, more broadly, shows that minor sequence variations can profoundly alter the active site of an enzyme. Lastly, we found that OXA-enzymes are inhibited by halogen ions, with iodide being the most potent inhibitor. The structure of OXA-163 in the presence of iodide shows that it changes the position of key active-site residues and prevents carboxylation of Lys73. This information may be utilized in the future development of class D inhibitors considering that the carboxylation of Lys73 is essential for the function of these enzymes.

AUTHOR INFORMATION

Corresponding Author

*Department of Pharmacology, Baylor College of Medicine, One Baylor Plaza, Houston, TX 77030. E-mail: timothyp@bcm.edu. Telephone: (713) 798-5609.

Funding

This work was supported by National Institutes of Health Grant AI32956 to T.P. B.V.V.P. acknowledges support from the Robert Welch Foundation (Q1279). The Berkeley Center for Structural Biology is supported in part by the National Institutes of Health, National Institute of General Medical Sciences, and the Howard Hughes Medical Institute. The Advanced Light Source is supported by the Director, Office of Science, Office of Basic Energy Sciences, of the U.S. Department of Energy under Contract DE-AC02-05CH1123. V.S. is supported by National Institute of Allergy and Infectious Diseases Training Grant T32 AI55449.

Notes

The authors declare no competing financial interest.

ACKNOWLEDGMENTS

We thank Hiram F. Gilbert for discussions and comments on the manuscript.

REFERENCES

(1) Pfeifer, Y., Cullik, A., and Witte, W. (2010) Resistance to cephalosporins and carbapenems in Gram-negative bacterial pathogens. *Int. J. Med. Microbiol. 300*, 371−379.

(2) McKenna, M. (2013) Antibiotic resistance: The last resort. *Nature 499*, 394−396.

(3) Lewis, K. (2013) Platforms for antibiotic discovery. *Nat. Rev. Drug Discovery 12*, 371−387.

(4) Nordmann, P., Dortet, L., and Poirel, L. (2012) Carbapenem resistance in Enterobacteriaceae: Here is the storm! *Trends Mol. Med. 18*, 263−272.

(5) Garbati, M. A., and Al Godhair, A. I. (2013) The growing resistance of *Klebsiella pneumoniae*; the need to expand our

antibiogram: Case report and review of the literature. *African Journal of Infectious Disease 7*, 8−10.
(6) Guh, A. Y., Limbago, B. M., and Kallen, A. J. (2014) Epidemiology and prevention of carbapenem-resistant Enterobacteriaceae in the United States. *Expert Rev. Anti-Infect. Ther. 12*, 565−580.
(7) Martinez-Martinez, L., and Gonzalez-Lopez, J. J. (2014) Carbapenemases in Enterobacteriaceae: Types and molecular epidemiology. *Enfermedades Infecciosas y Microbiología Clínica 32* (Suppl. 4), 4−9.
(8) Gutkind, G. O., Di Conza, J., Power, P., and Radice, M. (2013) β-Lactamase-mediated resistance: A biochemical, epidemiological and genetic overview. *Curr. Pharm. Des. 19*, 164−208.
(9) Drawz, S. M., and Bonomo, R. A. (2010) Three decades of β-lactamase inhibitors. *Clin. Microbiol. Rev. 23*, 160−201.
(10) Rice, L. B. (2012) Mechanisms of resistance and clinical relevance of resistance to β-lactams, glycopeptides, and fluoroquinolones. *Mayo Clin. Proc. 87*, 198−208.
(11) Therrien, C., and Levesque, R. C. (2000) Molecular basis of antibiotic resistance and β-lactamase inhibition by mechanism-based inactivators: Perspectives and future directions. *FEMS Microbiol. Rev. 24*, 251−262.
(12) Ambler, R. P. (1980) The structure of β-lactamases. *Philos. Trans. R. Soc., B 289*, 321−331.
(13) Bush, K. (1998) Metallo-β-lactamases: A class apart. *Clin. Infect. Dis. 27* (Suppl. 1), S48−S53.
(14) Gniadkowski, M. (2008) Evolution of extended-spectrum β-lactamases by mutation. *Clin. Microbiol. Infect. 14* (Suppl. 1), 11−32.
(15) Bush, K., and Jacoby, G. A. (2010) Updated functional classification of β-lactamases. *Antimicrob. Agents Chemother. 54*, 969−976.
(16) Papp-Wallace, K. M., Endimiani, A., Taracila, M. A., and Bonomo, R. A. (2011) Carbapenems: Past, present, and future. *Antimicrob. Agents Chemother. 55*, 4943−4960.
(17) Leonard, D. A., Bonomo, R. A., and Powers, R. A. (2013) Class D β-lactamases: A reappraisal after five decades. *Acc. Chem. Res. 46*, 2407−2415.
(18) Poirel, L., Naas, T., and Nordmann, P. (2010) Diversity, epidemiology, and genetics of class D β-lactamases. *Antimicrob. Agents Chemother. 54*, 24−38.
(19) Lahiri, S. D., Mangani, S., Jahic, H., Benvenuti, M., Durand-Reville, T. F., De Luca, F., Ehmann, D. E., Rossolini, G. M., Alm, R. A., and Docquier, J. D. (2015) Molecular Basis of Selective Inhibition and Slow Reversibility of Avibactam against Class D Carbapenemases: A Structure-Guided Study of OXA-24 and OXA-48. *ACS Chem. Biol. 10*, 591−600.
(20) Golemi, D., Maveyraud, L., Vakulenko, S., Samama, J. P., and Mobashery, S. (2001) Critical involvement of a carbamylated lysine in catalytic function of class D β-lactamases. *Proc. Natl. Acad. Sci. U.S.A. 98*, 14280−14285.
(21) Li, J., Cross, J. B., Vreven, T., Meroueh, S. O., Mobashery, S., and Schlegel, H. B. (2005) Lysine carboxylation in proteins: OXA-10 β-lactamase. *Proteins 61*, 246−257.
(22) Baurin, S., Vercheval, L., Bouillenne, F., Falzone, C., Brans, A., Jacquamet, L., Ferrer, J. L., Sauvage, E., Dehareng, D., Frere, J. M., Charlier, P., Galleni, M., and Kerff, F. (2009) Critical role of tryptophan 154 for the activity and stability of class D β-lactamases. *Biochemistry 48*, 11252−11263.
(23) Paetzel, M., Danel, F., de Castro, L., Mosimann, S. C., Page, M. G., and Strynadka, N. C. (2000) Crystal structure of the class D β-lactamase OXA-10. *Nat. Struct. Biol. 7*, 918−925.
(24) Heritier, C., Poirel, L., Aubert, D., and Nordmann, P. (2003) Genetic and functional analysis of the chromosome-encoded carbapenem-hydrolyzing oxacillinase OXA-40 of *Acinetobacter baumannii*. *Antimicrob. Agents Chemother. 47*, 268−273.
(25) Vercheval, L., Bauvois, C., di Paolo, A., Borel, F., Ferrer, J. L., Sauvage, E., Matagne, A., Frere, J. M., Charlier, P., Galleni, M., and Kerff, F. (2010) Three factors that modulate the activity of class D β-lactamases and interfere with the post-translational carboxylation of Lys70. *Biochem. J. 432*, 495−504.
(26) Bush, K., Jacoby, G. A., and Medeiros, A. A. (1995) A functional classification scheme for β-lactamases and its correlation with molecular structure. *Antimicrob. Agents Chemother. 39*, 1211−1233.
(27) Bush, K. (2013) Proliferation and significance of clinically relevant β-lactamases. *Ann. N.Y. Acad. Sci. 1277*, 84−90.
(28) Poirel, L., Potron, A., and Nordmann, P. (2012) OXA-48-like carbapenemases: The phantom menace. *J. Antimicrob. Chemother. 67*, 1597−1606.
(29) Walther-Rasmussen, J., and Hoiby, N. (2006) OXA-type carbapenemases. *J. Antimicrob. Chemother. 57*, 373−383.
(30) Kamolvit, W., Derrington, P., Paterson, D. L., and Sidjabat, H. E. (2015) A Case of IMP-4-, OXA-421-, OXA-96-, and CARB-2-Producing *Acinetobacter pittii* Sequence Type 119 in Australia. *J. Clin. Microbiol. 53*, 727−730.
(31) Livermore, D. M. (2009) Has the era of untreatable infections arrived? *J. Antimicrob. Chemother. 64* (Suppl.1), i29−i36.
(32) Oueslati, S., Nordmann, P., and Poirel, L. (2015) Heterogeneous hydrolytic features for OXA-48-like β-lactamases. *J. Antimicrob. Chemother.*, DOI: 10.1093/jac/dku524.
(33) Poirel, L., Heritier, C., Tolun, V., and Nordmann, P. (2004) Emergence of oxacillinase-mediated resistance to imipenem in *Klebsiella pneumoniae*. *Antimicrob. Agents Chemother. 48*, 15−22.
(34) Docquier, J. D., Calderone, V., De Luca, F., Benvenuti, M., Giuliani, F., Bellucci, L., Tafi, A., Nordmann, P., Botta, M., Rossolini, G. M., and Mangani, S. (2009) Crystal structure of the OXA-48 β-lactamase reveals mechanistic diversity among class D carbapenemases. *Chem. Biol. 16*, 540−547.
(35) Poirel, L., Castanheira, M., Carrer, A., Rodriguez, C. P., Jones, R. N., Smayevsky, J., and Nordmann, P. (2011) OXA-163, an OXA-48-related class D β-lactamase with extended activity toward expanded-spectrum cephalosporins. *Antimicrob. Agents Chemother. 55*, 2546−2551.
(36) Abdelaziz, M. O., Bonura, C., Aleo, A., El-Domany, R. A., Fasciana, T., and Mammina, C. (2012) OXA-163-producing *Klebsiella pneumoniae* in Cairo, Egypt, in 2009 and 2010. *J. Clin. Microbiol. 50*, 2489−2491.
(37) Smith, C. A., Antunes, N. T., Toth, M., and Vakulenko, S. B. (2014) Crystal structure of carbapenemase OXA-58 from *Acinetobacter baumannii*. *Antimicrob. Agents Chemother. 58*, 2135−2143.
(38) Maveyraud, L., Golemi, D., Kotra, L. P., Tranier, S., Vakulenko, S., Mobashery, S., and Samama, J. P. (2000) Insights into class D β-lactamases are revealed by the crystal structure of the OXA10 enzyme from *Pseudomonas aeruginosa*. *Structure 8*, 1289−1298.
(39) De Luca, F., Benvenuti, M., Carboni, F., Pozzi, C., Rossolini, G. M., Mangani, S., and Docquier, J. D. (2011) Evolution to carbapenem-hydrolyzing activity in noncarbapenemase class D β-lactamase OXA-10 by rational protein design. *Proc. Natl. Acad. Sci. U.S.A. 108*, 18424−18429.
(40) Sosa-Peinado, A., Mustafi, D., and Makinen, M. W. (2000) Overexpression and biosynthetic deuterium enrichment of TEM-1 β-lactamase for structural characterization by magnetic resonance methods. *Protein Expression Purif. 19*, 235−245.
(41) Gasteiger, E., Hoogland, C., Gattiker, A., Duvaud, S., Wilkins, M. R., Appel, R. D., and Bairoch, A. (2005) Protein Identification and Analysis Tools on the ExPASy Server. In *The Proteomics Protocols Handbook* (Walker, J. M., Ed.) pp 571−607, Humana Press, Totowa, NJ.
(42) Stojanoski, V., Chow, D. C., Hu, L., Sankaran, B., Gilbert, H. F., Prasad, B. V., and Palzkill, T. (2015) A Triple Mutant in the Ω-loop of TEM-1 β-Lactamase Changes the Substrate Profile via a Large Conformational Change and an Altered General Base for Catalysis. *J. Biol. Chem. 290*, 10382−10394.
(43) Wahl, R. C. (1994) The calculation of initial velocity from product progress curves when $[S] \ll K_m$. *Anal. Biochem. 219*, 383−384.
(44) Poirel, L., Girlich, D., Naas, T., and Nordmann, P. (2001) OXA-28, an extended-spectrum variant of OXA-10 β-lactamase from *Pseudomonas aeruginosa* and its plasmid- and integron-located gene. *Antimicrob. Agents Chemother. 45*, 447−453.

(45) Winn, M. D., Ballard, C. C., Cowtan, K. D., Dodson, E. J., Emsley, P., Evans, P. R., Keegan, R. M., Krissinel, E. B., Leslie, A. G., McCoy, A., McNicholas, S. J., Murshudov, G. N., Pannu, N. S., Potterton, E. A., Powell, H. R., Read, R. J., Vagin, A., and Wilson, K. S. (2011) Overview of the CCP4 suite and current developments. *Acta Crystallogr. D67*, 235−242.
(46) Battye, T. G., Kontogiannis, L., Johnson, O., Powell, H. R., and Leslie, A. G. (2011) iMOSFLM: A new graphical interface for diffraction-image processing with MOSFLM. *Acta Crystallogr. D67*, 271−281.
(47) Vagin, A., and Teplyakov, A. (2010) Molecular replacement with MOLREP. *Acta Crystallogr. D66*, 22−25.
(48) Adams, P. D., Afonine, P. V., Bunkoczi, G., Chen, V. B., Davis, I. W., Echols, N., Headd, J. J., Hung, L. W., Kapral, G. J., Grosse-Kunstleve, R. W., McCoy, A. J., Moriarty, N. W., Oeffner, R., Read, R. J., Richardson, D. C., Richardson, J. S., Terwilliger, T. C., and Zwart, P. H. (2010) PHENIX: A comprehensive Python-based system for macromolecular structure solution. *Acta Crystallogr. D66*, 213−221.
(49) Emsley, P., Lohkamp, B., Scott, W. G., and Cowtan, K. (2010) Features and development of Coot. *Acta Crystallogr. D66*, 486−501.
(50) Terwilliger, T. C., Grosse-Kunstleve, R. W., Afonine, P. V., Moriarty, N. W., Zwart, P. H., Hung, L. W., Read, R. J., and Adams, P. D. (2008) Iterative model building, structure refinement and density modification with the PHENIX AutoBuild wizard. *Acta Crystallogr. D64*, 61−69.
(51) Afonine, P. V., Grosse-Kunstleve, R. W., Echols, N., Headd, J. J., Moriarty, N. W., Mustyakimov, M., Terwilliger, T. C., Urzhumtsev, A., Zwart, P. H., and Adams, P. D. (2012) Towards automated crystallographic structure refinement with phenix.refine. *Acta Crystallogr. D68*, 352−367.
(52) Vagin, A. A., Steiner, R. A., Lebedev, A. A., Potterton, L., McNicholas, S., Long, F., and Murshudov, G. N. (2004) REFMAC5 dictionary: Organization of prior chemical knowledge and guidelines for its use. *Acta Crystallogr. D60*, 2184−2195.
(53) Bolton, E., Wang, Y., Thiessen, P. A., and Bryant, S. H. (2008) PubChem: Integrated Platform of Small Molecules and Biological Activities. In *Annual Reports in Computational Chemistry*, Chapter 12, American Chemical Society, Washington, DC.
(54) Trott, O., and Olson, A. J. (2010) AutoDock Vina: Improving the speed and accuracy of docking with a new scoring function, efficient optimization, and multithreading. *J. Comput. Chem. 31*, 455−461.
(55) Morris, G. M., Goodsell, D. S., Halliday, R. S., Huey, R., Hart, W. E., Belew, R. K., and Olson, A. J. (1998) Automated Docking Using a Lamarckian Genetic Algorithm and and Empirical Binding Free Energy Function. *J. Comput. Chem. 19*, 1639−1662.
(56) Berman, H. M., Westbrook, J., Feng, Z., Gilliland, G., Bhat, T. N., Weissig, H., Shindyalov, I. N., and Bourne, P. E. (2000) The Protein Data Bank. *Nucleic Acids Res. 28*, 235−242.
(57) Krissinel, E., and Henrick, K. (2004) Secondary-structure matching (SSM), a new tool for fast protein structure alignment in three dimensions. *Acta Crystallogr. D60*, 2256−2268.
(58) Pettersen, E. F., Goddard, T. D., Huang, C. C., Couch, G. S., Greenblatt, D. M., Meng, E. C., and Ferrin, T. E. (2004) UCSF Chimera: A visualization system for exploratory research and analysis. *J. Comput. Chem. 13*, 1605−1612.
(59) Docquier, J. D., Benvenuti, M., Calderone, V., Giuliani, F., Kapetis, D., De Luca, F., Rossolini, G. M., and Mangani, S. (2010) Crystal structure of the narrow-spectrum OXA-46 class D β-lactamase: Relationship between active-site lysine carbamylation and inhibition by polycarboxylates. *Antimicrob. Agents Chemother. 54*, 2167−2174.
(60) Gomez, S., Pasteran, F., Faccone, D., Bettiol, M., Veliz, O., De Belder, D., Rapoport, M., Gatti, B., Petroni, A., and Corso, A. (2013) Intrapatient emergence of OXA-247: A novel carbapenemase found in a patient previously infected with OXA-163-producing *Klebsiella pneumoniae*. *Clin. Microbiol. Infect. 19*, E233−E235.
(61) Pernot, L., Frenois, F., Rybkine, T., L'Hermite, G., Petrella, S., Delettre, J., Jarlier, V., Collatz, E., and Sougakoff, W. (2001) Crystal structures of the class D β-lactamase OXA-13 in the native form and in complex with meropenem. *J. Mol. Biol. 310*, 859−874.
(62) Abendroth, J., Gardberg, A. S., Robinson, J. I., Christensen, J. S., Staker, B. L., Myler, P. J., Stewart, L. J., and Edwards, T. E. (2011) SAD phasing using iodide ions in a high-throughput structural genomics environment. *J. Struct. Funct. Genomics 12*, 83−95.
(63) Gibb, C. L., and Gibb, B. C. (2011) Anion binding to hydrophobic concavity is central to the salting-in effects of Hofmeister chaotropes. *J. Am. Chem. Soc. 133*, 7344−7347.
(64) Fox, J. M., Kang, K., Sherman, W., Heroux, A., Sastry, G. M., Baghbanzadeh, M., Lockett, M. R., and Whitesides, G. M. (2015) Interactions between Hofmeister Anions and the Binding Pocket of a Protein. *J. Am. Chem. Soc. 137*, 3859−3866.
(65) Schneider, K. D., Karpen, M. E., Bonomo, R. A., Leonard, D. A., and Powers, R. A. (2009) The 1.4 Å crystal structure of the class D β-lactamase OXA-1 complexed with doripenem. *Biochemistry 48*, 11840−11847.
(66) Rankin, B. M., and Ben-Amotz, D. (2013) Expulsion of ions from hydrophobic hydration shells. *J. Am. Chem. Soc. 135*, 8818−8821.
(67) Politzer, P., Murray, J. S., and Bulat, F. A. (2010) Average local ionization energy: A review. *J. Mol. Model. 16*, 1731−1742.